AUT Journal of Mechanical Engineering

AUT J. Mech. Eng., 7(2) (2023) 131-154
DOI: 10.22060/ajme.2023.21980.6051

Ferrofluid Injection and Applied Magnetic Field Influences on the Characteristics of Flow Over a Cylinder

Saber Yekani Motlagh, Iman Tolouie , Ehsan Tolouie, Farrokh Mobadersani*

Faculty of Mechanical Engineering, Urmia University of Technology (UUT), Urmia, Iran

ABSTRACT: The present article presents an innovative method to reduce drag in flow over a cylinder by using Kelvin force. In contrast to the previous works, there is no need to move or additional geometry parts. For this purpose, nanofluid is injected from gaps embedded over the circular cylinder surface. Moreover, the heat transfer rate has been evaluated over the rigidly fixed cylinder surface. In this study, flow and heat transfer characteristics are investigated by the open-source code of Openfoam, under the effect of the induced magnetic field of a single electric current carrier wire. The modified model of Buongiorno that contains the magnetophoresis term is utilized for the two-phase modeling of ferrofluid flow. For discretization of the governing unsteady equations including conservation laws of mass, volume fraction transport, and momentum equations that contain the ferro-hydrodynamics force as a source term, the Finite volume method, and PISO algorithm are considered. The drag coefficient, entropy generation, Nusselt number, streamlines, and temperature contours are computed for three Reynolds numbers of 120,150, and 180. It is obtained that, the presence of the magnetic field at various volume fractions has significant effects on these parameters. For instance, by increasing the magnetic intensity (B) from 0 to 0.002 T, the pressure drag coefficient, the total entropy generation, and the Nusselt number are reduced by about 153%, 11.76%, and 17.24%, respectively.

Review History:

Received: Nov. 30, 2022
Revised: Mar. 18, 2023
Accepted: Sep. 02, 2023
Available Online: Sep. 12, 2023

Keywords:

Vortex shedding
Flow control
Heat transfer
Ferrohydrodynamics (FHD)
Boungiorno model
Entropy generation

1- Introduction

The concept of nanofluid includes the suspensions containing nonmetallic and metal nanoparticles which are provided by the distribution of nano dimension particles in fluids such as water, Ethylene, blood, oil, etc. Nanofluids are the new generation of fluids with high potential in industrial applications such as heat exchangers [1-4], condensers [5], drug delivery [6-9], and so on. The range of the diameter of the particles used in nanofluids is restricted from 1nm to 100nm.

Investigation of heat transfer changes has become a critical issue for researchers, which encourage them to study in various aspects of heat transfer and flow control over bluff bodies. Tsai and Chein. [10] by using carbon nano tube/water and copper/water nanofluid, analytically investigated the efficiency of the microchannel heat sink. Dulhani et al. [11] conducted the study of heat transfer characteristic and mixed convective flow around a square obstacle for various angles of incidence. Bayat et al. [12] studied the effect of adding aluminum oxide nanoparticles to pure water on Nusselt number, drag and lift coefficients. Their studies performed for laminar flow at various volume fractions and Reynolds numbers. Their results showed that the addition of aluminum oxide nanoparticles has an irrefutable effect on the increment of heat transfer rate and drag coefficient. Based on their results the drag coefficient increases 1 to 4 percent by increasing the volume fraction of iron oxide Nanoparticles. Bhinder et al. [13] numerically investigated the fluid dynamic and force convective heat transfer around a semicircular obstacle. They concluded that increasing the angle of incident causes the enhancement of streamline curvature. Valipour et al. [14] studied the effect of utilizing Al_2O_3 / H_2O nanofluid on the fluid flow and forced convective heat transfer over a square obstacle at low Reynolds numbers. Their results showed that the addition of nanoparticles to the base fluid, in the inverse pressure gradient case, causes the increment of pressure coefficient. The effect of the different orientation of triangle obstacle on the heat transfer rate of Al_2O_3 / H_2O Nanofluid is investigated by Esfahani et al. [15]. It can be seen from their results that maximum enhancement of heat transfer rate is for the side facing flow and minimum is for vertex facing flow. Since the flow separation and wake region behavior causes structural vibrations, these phenomena are unpleasant from the industrial perspective. For instance, the collapse of offshore structures, the vibration of pipelines, chimneys near tall Buildings, skyscrapers and so many other damages can be the examples of these phenomena. Therefore, researchers struggling to find out the ways to decrease the unsteady hydrodynamic forces that applying to structures. Generally, common methods for controlling the structure of

*Corresponding author's email: f.mobadersani@mee.uut.ac.ir

the wake region and the oscillation of vortices are categorized into: suction/blowing, synthetic jet, electromagnetic forcing, rotation, forced oscillations, travelling wave wall, and etc. Prabir et al. [16] considered a rigid splitter at the back face of a cylinder and investigated the structure of the wake region and drag changes. Travelling wavy wall effect on friction and pressure drag coefficients on a cylinder in 2D simulations are reported by Feng et al. [17]. Gao et al. [18] experimentally studied the flow around a cylinder with suction/blowing structures on the surface of the cylinder and reported the maximum drag reduction. Also, the researchers conducted other passive methods such as modification of the geometry and using external small parts, vertex manufacturers, flaps and so on [19-22] on the flow controlling phenomenon. Permeable plates are attached by Ozkan and Akilli [23] to pull off the length of vortexes. Their studies were useful in reducing of the fluctuations in the wake region. The significant effect of the secondary cylinder which placed in the wake region of the main cylinder has been demonstrated by Mittal and Raghuvanshi [24]. Their suggested method was useful at the development of a local favorable pressure gradient in the wake region for low Reynolds numbers. The effect of surface roughness on postponing the separation of the boundary layer was carried out experimentally by Zhou et al. [25]. Their results revealed that surface roughness leads to a rapid transition from laminar to turbulent regime that reduces the lift and drag coefficient. Chen et al. [26] utilized the flow suction method to suppress the vortex-induced vibration of the circular obstacle. Their experiments were conducted for four different flow suction rates to find the optimum suction rate. They succeeded in declining the unsteady forces and amplitude of the oscillation was also decreased. The small counter-rotating cylinder has been utilized by Schulmeister et al. [27] to reduce the drag coefficient of the main cylinder. It can be perceived from their results that the use of a secondary counter-rotating cylinder is beneficent due to shortening the recirculation length and narrowing the mean wake. One of the most widely used alternative methods for controlling the flow is magnetic hydrodynamics (MHD) in which the Lorentz volumetric force is generated due to the application of magnetic fields in electrically conducting fluids. MHD flow over a circular cylinder was studied by Grigoriadis et al. [28]. They utilized the immersed boundary method to show the effectivity of MHD flow control method in decreasing the amount of drag coefficient. Zhang et al. [29] tried to suppress the vortex-induced vibration of a 2D moving circular cylinder by applying the Lorentz forces. Their work showed the impact of Lorentz force on lift force, the vortex induced lift force and the phase angles among the obstacle displacement. Rezaie and Norouzi [30] numerically investigated magnetohydrodynamics flow of non-Newtonian fluid over a circular cylinder. Their study showed that the amplitude of the fluctuation of the drag and lift coefficient decreases due to the presence of strong magnetic field, and controlling vortex shedding in shear-thinning fluid requires the insertion of the substantial value of the magnetic field. In spite of the magnetohydrodynamics, that recognized as one of the useful methods of flow control and flow stabilization, Ferrohydrodynamics (FHD) are also considered due to the high magnetic saturation and poor electrical conductivity of Nanofluids [31-36]. Numerical study of the magnetic drug delivery to the targeted tissue was done by Yekani and Deyhim [37]. Their investigation was carried out on three different types of magnetic sources under the influence of different electrical currents. According to their results, the Kelvin force generates vortices inside fluid domain. These vortices prevent the drug from entering the target tissue and also, they stated that, drug concentration in tissue increases by augmentation of particles injection. Sharifi et al. [38] utilized the principles of ferrohydrodynamics to study the effects of various inclination angles of two inclined rectangular permanent magnets and saturated magnetization on heat transfer and flow characteristics of blood flow. According to their results, C_f and Nu number decrease due to increasing the inclination angle of magnets. Moreover, overall energy loss, increases by the increment of saturated magnetization. Magnetic drug targeting was conducted by Sharifi et al. [39] in aneurysm vessel at Re=200 and drug was coated on Fe_3O_4 / H_2O nanoparticles. Their studies showed that the duration of the presence of the drugs on the target tissue affected by three mechanisms includes the formation of a droplet of drug, vortex and creeping flow in entrance regions of aneurysm vessel.

The flow control on a body in all the previous works carried out, utilizing common ways such as: suction/blowing, synthetic jet, rotation, forced oscillations, etc. The flow-controlling efficiency of these methods is restricted and also their implementation may need the addition of auxiliary moving or fixed parts. In the present work, flow control on a cylinder was carried out with the injection of ferrofluids and the Kelvin force induced by the electric current carrying wire without any additional moving of fixed parts, for the first time. Moreover, detailed results to investigate effective parameters such as the volume fraction, intensity of magnetite field on the pressure coefficient, Strouhal number, drag coefficient, and entropy generation, are investigated for three Reynolds numbers of 120, 150, and 180.

1- 1- Problem description

The problem under study is for a fixed 2D circular cylinder with a diameter of 1cm which is surrounded by a rectangular domain. The schematic view of the problem is illustrated in Fig.1. The side edges are supposed to be open boundaries to neglect wall effects. The inlet and outlet distances to the cylinder center are 10 and 20 times of the cylinder diameter (D), respectively. The distance from the center of the cylinder to the side walls is 10 D. Pure water flows over the circular cylinder with a temperature of 309 K and free stream velocity of U_∞. The circular cylinder maintained at a constant temperature of 350 K. Fe_3O_4 / H_2O nanofluid is injected from gaps of 12^o arc length which are located at the top and bottom of the cylinder. The nanoparticle's diameter is assumed to be 10 nm. To apply the magnetic field to a ferrofluid, a wire that carries an electrical current is placed

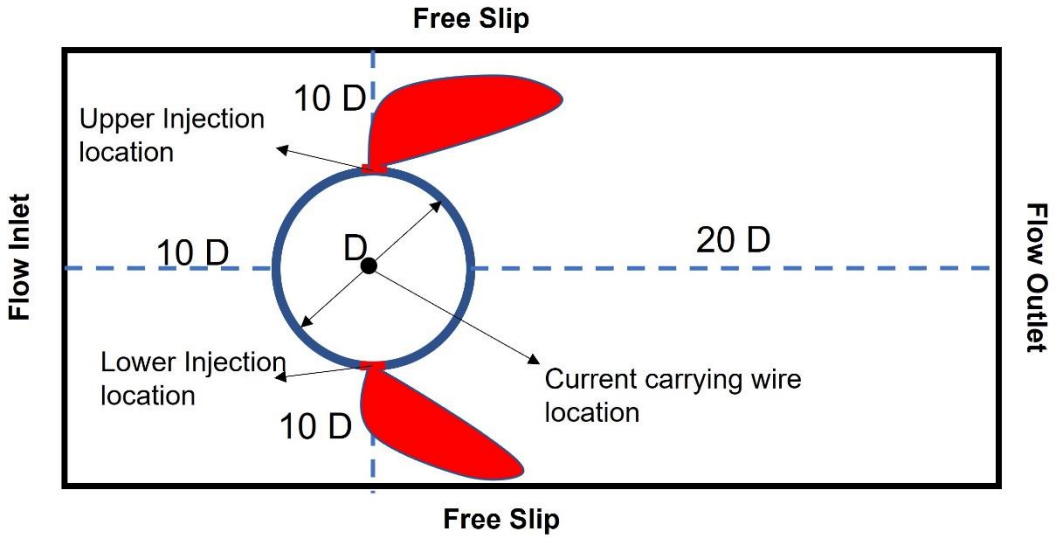

Fig. 1. Schematic description of the problem.

at the center of the cylinder. The study is conducted for three different Reynolds numbers in a laminar flow regime in the periodic vortex shedding range (Re=120, Re=150, Re=180).

1- 2- Dimensional form of governing equations and boundary conditions

The governing equations for the two-dimensional unsteady flow of an incompressible and Newtonian fluid are continuity, momentum, energy, and nanoparticle volume fraction that can be written as below [36, 37]:

Continuity equation:

$$\nabla.\mathbf{V} = 0 \tag{1}$$

Where **V** is the velocity vector.

Momentum equation:

$$\rho_{nf}\left(\frac{\partial \mathbf{V}}{\partial t} + \mathbf{V}.\nabla\mathbf{V}\right) = -\nabla p + \nabla.(\mu_{nf}\nabla\mathbf{V}) + \mu_0\mathbf{M}.\nabla H \tag{2}$$

Where $\mu_0\mathbf{M}.\nabla H$ is the Kelvin force vector which derives from the magnetic source. The direction of Kelvin force, that applies to the magnetic nanofluids is towards the location of the wire. In other words, it causes the attraction of magnetic nanofluid to the cylinder surface. Effective dynamic viscosity, the density of nanofluid, pressure, magnetization fields, and the magnetic field intensity are demonstrated by μ_{nf} , ρ_{nf} , p , $\mathbf{M}$ and H , respectively. As aforementioned, in the present work, a current-carrying wire is considered as a magnetic source that applies a non-uniform magnetic field to the computational domain with the intensity of the following components [31]:

$$H_x = \frac{I}{2\pi}\frac{1}{(x-a)^2+(y-b)^2}(y-b) \tag{3}$$

$$H_y = \frac{-I}{2\pi}\frac{1}{(x-a)^2+(y-b)^2}(x-a) \tag{4}$$

Where point (a ,b) demonstrates the wire locations. Magnetization ($\mathbf{M}$) could be written as follows [31]:

$$\mathbf{M} = M_s L(\xi) \tag{5}$$

In which M_s is the saturation magnetization of magnetic nanofluid, L is the Langevin function, and $\hat{\mathbf{i}}$ is the Langevin parameter, which is as follows [31]:

$$M_s = \frac{6\varphi}{\pi {d_p}^3} m_p \tag{6}$$

$$L(\xi) = \coth(\xi) - \frac{1}{\xi} \tag{7}$$

$$\xi = \frac{\mu_0 m_p \mathbf{H}}{k_B T} \tag{8}$$

In the above equations, d_p represent the magnetic nanoparticles diameter. k_B and T demonstrate Boltzmann's constant and absolute temperature field, respectively. For evaluating the magnetic moment of the iron oxide nanoparticles, the following equation is used.

$$m_p = \frac{4\mu_B \pi d_p^{\,3}}{6\times 91.25\times 10^{-30}} \tag{9}$$

μ_B represents Bohr's Magneton and its value is 9.27 The Langevin function can be approximated as [31]:

$$L(\xi) = \coth(\xi) - \frac{1}{\xi} = \frac{\xi}{3} \tag{10}$$

According to the above equations, the magnetization of magnetic nanofluid can be expressed as follows:

$$\mathbf{M} = \chi(\varphi, T)\mathbf{H} \tag{11}$$

χ in the above equation is called as magnetic susceptibility and it is calculated from the following relation:

$$\chi = \frac{2\varphi\mu_0 m_p^{\,2}}{\pi d_p^{\,3} k_B T} \tag{12}$$

Energy equation [40]:

$$(\rho_{nf}(\frac{\partial T}{\partial t} + \mathbf{V}.\nabla T) = \nabla.(k_{nf}\nabla T) - (\rho C_{p\,np}\mathbf{J_p}.\nabla T) \tag{13}$$

Volume fraction equation [40]:

$$\frac{\partial \varphi}{\partial t} + \mathbf{V}.\nabla\varphi = -\frac{1}{\rho_{np}}(\nabla.\mathbf{J_p}) \tag{14}$$

Where $C_{p\,nf}$, k_{nf}, $C_{p\,np}$, φ, $\mathbf{J_p}$ and ρ_{nf} are the nanofluid heat capacity, nanofluid thermal conductivity, nanoparticles heat capacity, volume fraction, mass flux of nanoparticles, and density of nanoparticles, respectively. Based on the Buongiorno model [40], $\mathbf{J_p}$ is only affected by the thermophoresis effect ($\mathbf{J}_{p,T}$, Eq. 15) and Brownian motion ($\mathbf{J}_{p,B}$, Eq. 16). The last term in Eq.13 states that the heat transfer can occur by virtue of nanoparticles diffusion. Despite the Buongiorno model which has not included the effect of the magnetic force, the magnetophoresis term, $\mathbf{J}_{p,M}$ has been introduced to the Buongiorno model in the present article as [40]:

$$\mathbf{J}_{p,T} = -\rho_{np} D_T \nabla T \tag{15}$$

$$\mathbf{J}_{p,B} = -\rho_{np} D_B \nabla\varphi \tag{16}$$

$$\mathbf{J}_{p,M} = -\rho_{np} D_B \frac{\varphi}{H}\xi L(\xi)\nabla H \tag{17}$$

$$\mathbf{J}_p = \mathbf{J}_{p,T} + \mathbf{J}_{p,B} + \mathbf{J}_{p,M} \tag{18}$$

D_B and D_T are the Brownian diffusion and thermophoresis coefficients, respectively. These terms can be written as following equations:

$$D_T = 0.26\frac{k_f}{2k_f + k_p}\frac{\mu_f}{\rho_f}\varphi \tag{19}$$

$$D_B = \frac{k_B T}{3\pi\mu_f d_p} \tag{20}$$

The closed form of the volume fraction transport equation is concluded by substituting the nanoparticle's mass flux from Eq. (18) into Eq. (14) [40].

$$\rho_{np}(\frac{\partial\varphi}{\partial t} + \mathbf{V}.\nabla\varphi) = \nabla.(\rho_{np} D_B \nabla\varphi) + \nabla.(\rho_{np} D_T \frac{\nabla T}{T}) - \nabla.(\rho_{np} D_B (\frac{\varphi}{H})\xi L(\xi)) \tag{21}$$

According to the problem definition, proper boundary conditions can be supposed as follows.

Fluid enters the domain with constant velocity, which is adjusted based on Re and a constant temperature of 309 K. In the outlet, zero gradient boundary condition is applied to the volume fraction equation whereas pressure value is assumed to be zero at the outlet.

Zero gradient boundary conditions for pressure and slip conditions for velocity are used for upper and lower boundaries.

The cylinder surface is maintained at a constant temperature of 350 K. Nanofluid with a constant volume fraction of nanoparticles is injected from gaps located at the top and bottom of the cylinder with a temperate of 309K and $v = U/2$ (y component velocity), and also the no-slip and zero gradients are considered for velocity and pressure boundary conditions, respectively. The transport flux of nanoparticles is considered to be zero in the perpendicular direction to the impermeable walls surface, which will be as:

$$\mathbf{J}_p.\mathbf{n} = (\mathbf{J}_{p,B} + \mathbf{J}_{p,M} + \mathbf{J}_{p,T}).\mathbf{n} = 0 \tag{22}$$

n is the unit wall normal vector and after simplifications, the boundary condition at the walls will be:

$$\nabla\varphi.\mathbf{n} = (-\frac{D_T}{D_B}\nabla T + (\frac{\varphi}{H}\xi L(\xi)\nabla H).\mathbf{n} \tag{23}$$

To illustrate the results clearly, C_d, St, C_f, C_p and Nu_{avg} are defined by Eqs. (24)-(28). F_d In equation (24) is the corresponding drag force. f in equation (25) is the shedding frequency in Hz and p is static pressure that is used in Eq. (26). In all equations, the subscript infinity refers to free-stream (inlet velocity) values. The average Nusselt number is calculated by Eq. (28) over the cylinder surface by integrating the local Nusselt number.

$$C_d = \frac{F_d}{\frac{1}{2}\rho_\infty {U_\infty}^2 A} \tag{24}$$

$$St = \frac{fL}{V} \tag{25}$$

$$C_f = \frac{\tau_w}{\frac{1}{2}\rho_\infty {U_\infty}^2}, C_p = \frac{p - p_\infty}{\frac{1}{2}\rho_\infty {U_\infty}^2} \tag{26}$$

$$Nu_{ave} = \int \frac{k_{nf}}{k_f}\nabla^* T^*.\mathbf{n} \tag{27}$$

1- 3- Magnetic nanofluid properties

In the current work, the proposed formula of Brinkman [41] for a dilute suspension of spherical particles has been used to evaluate the nanofluid viscosity:

$$\mu_{nf} = \frac{\mu_f}{(1-\varphi)^{2.5}} \tag{28}$$

The density and specific heat of the nanofluid can be written as follows:

$$\rho_{nf} = \varphi\rho_{np} + (1-\varphi)\rho_f \tag{29}$$

$$(\rho C_p)_{nf} = \varphi(\rho C_p)_{np} + (1-\varphi)(\rho C_p)_f \tag{30}$$

As shown by Khanafer et al. [42], the thermal conductivity of the fluid generated by the Maxwell-Greens model has been calculated approximately by:

$$k_{nf} = k_f \frac{(-2\varphi(k_f - k_{np}) + 2k_f + k_{np})}{\varphi(k_f - k_{np}) + 2k_f + k_{np}} \tag{31}$$

Entropy generation is the amount of entropy which is produced in any irreversible processes, such as heat and mass transfer processes including chemical reaction, motion of bodies, heat loss, substances expanding or mixing, the local volumetric entropy generation rate with the convective heat transfer and viscous effects which can be calculated by:

$$\begin{aligned} S_{gen}''' &= \frac{k_{nf}}{T^2}((\frac{\partial T}{\partial x})^2 + (\frac{\partial T}{\partial y})^2) \\ &+ \frac{\mu_{nf}}{T}(2((\frac{\partial u}{\partial x})^2 + (\frac{\partial u}{\partial y})^2) \\ &+ ((\frac{\partial v}{\partial x})^2 + (\frac{\partial v}{\partial y})^2)) \end{aligned} \tag{32}$$

The first term of the above equation represents the entropy generation due to heat transfer and the second term is due to the fluid friction.

Thermo-physical properties of Fe_3O_4 magnetic nanoparticles and water are illustrated in Table 1.

2- Numerical method

In the current study, heat transfer and flow characteristics are obtained by solving governing equations by utilizing the developed form of the object-oriented C++ code. Pressure and velocity are linked by using the PISO-based finite volume method. For discretizing the diffusion terms of governing equations and interpolating the convective terms, the second-order central difference scheme and the upwind scheme are employed, respectively. To ensure of temporal accuracy and numerical stability Courant number of 0.5 is considered.

Table 1. Base fluid and Nanoparticles properties.

	ρ (kg/m^3)	k (W/m.K)	C_p (J/kg.K)
Fe_3O_4	5200	6	670
Water	993	0.628	4178

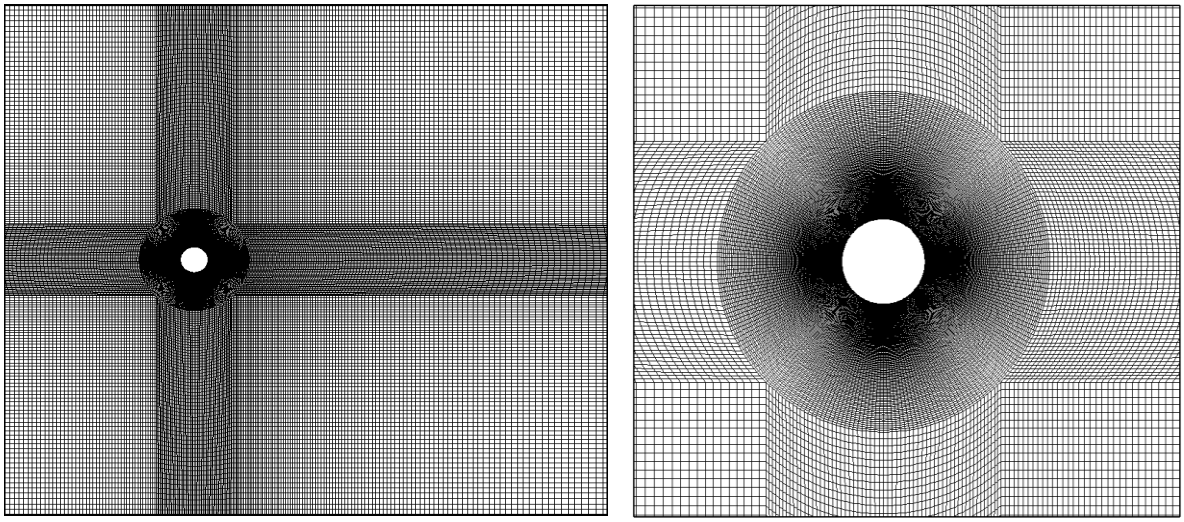

a *b*

Fig. 2. a) Non-uniform mesh distribution along the computational domain b) Mesh refinement near the cylinder surface.

2- 1- Grid independent study

As demonstrated in Fig. 2(a) two-dimensional structured mesh is generated for all cases. The mesh density due to the large gradient of pressure and velocity near the cylinder surface is enhanced. Mesh refinement near the surface of the cylinder is shown in Fig. 2(b). To achieve an accurate solution, a grid sensitivity analysis in the most critical condition is performed. Table 2 shows the four different grid densities. To ensure that the results are grid independent, the number of computational cells is increased to 105100 cells. Based on the differences in drag coefficient and Strouhal number between cases 3 and 4, 87600 mesh has been selected as the optimal mesh for all case studies.

2- 2- Validation

For benchmarking the authenticity of the numerical method, validation has been done with experimental and numerical studies in a wide range of Reynolds numbers. The present numerical values of the drag coefficient and the Strouhal numbers are compared with the compiled data of Zdrakovich [43] and measured data of Norberg [44] and Williamson [45] which is presented in Fig. 3. The comparison between the results indicates that reasonable conformity exists, with the mean root square error of 6.9% and ~6.33% to 7.64% for the drag coefficient and the Strouhal numbers, respectively. To verify the accuracy of the results, the surface pressure coefficient and skin friction coefficient have been compared with experimental and numerical studies as shown in Fig. 4. The results of the surface pressure coefficient for three Reynolds numbers of 60, 150, and 90 and the skin friction coefficient for four Reynolds numbers of 40, 60, 90 and 180 have been calculated. For detailed information, refer to [46] and [47] references. To ensure the code accuracy, further validation has been done for the average Nusselt number, as presented in table 3. Compared results are in close agreement with the results obtained by Zukauskas [48]. To verify the accuracy of using the current code to study FHD in the presence of a magnetic field, the results of the temperature field are compared with those of Song and Tagawa [49] in Fig.5. The problem studied in [49] is the magneto-convection phenomenon in a square cavity containing Oxygen. The cavity is heated differentially and the non-uniform magnetic field is applied by a permanent magnet. Furthermore, a comparison is performed by available cases of aneurysmal blood flow

Table 2. Grid sensitivity test on drag coefficient and Strouhal number.

Case	Cell Number	C_d	Error%	St	Error%
1	33600	1.3825	1.12	0.2037	0.589
2	54500	1.367	1.2	0.2025	2.27
3	87600	1.3505	0.22	0.1979	0.35
4	105100	1.3535		0.1972	

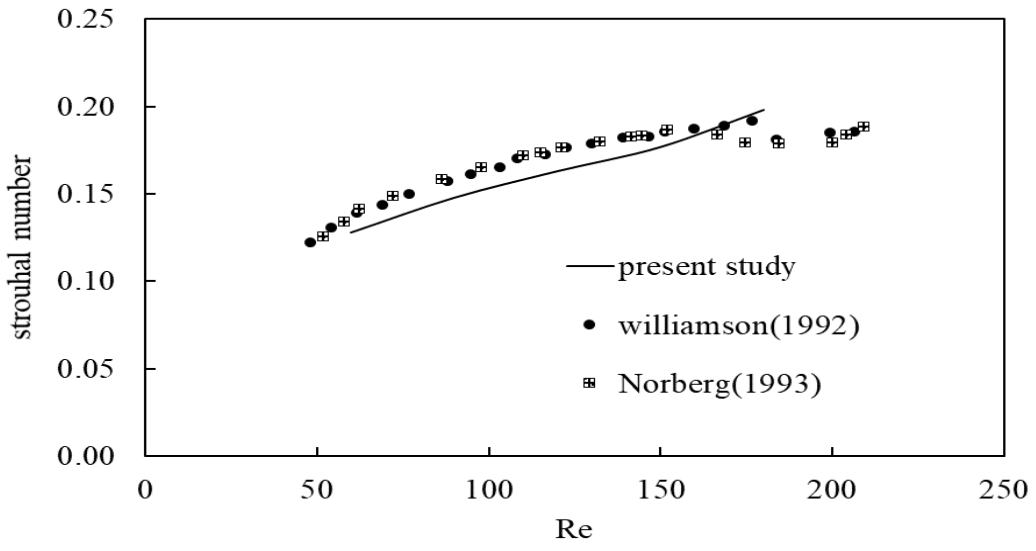

a

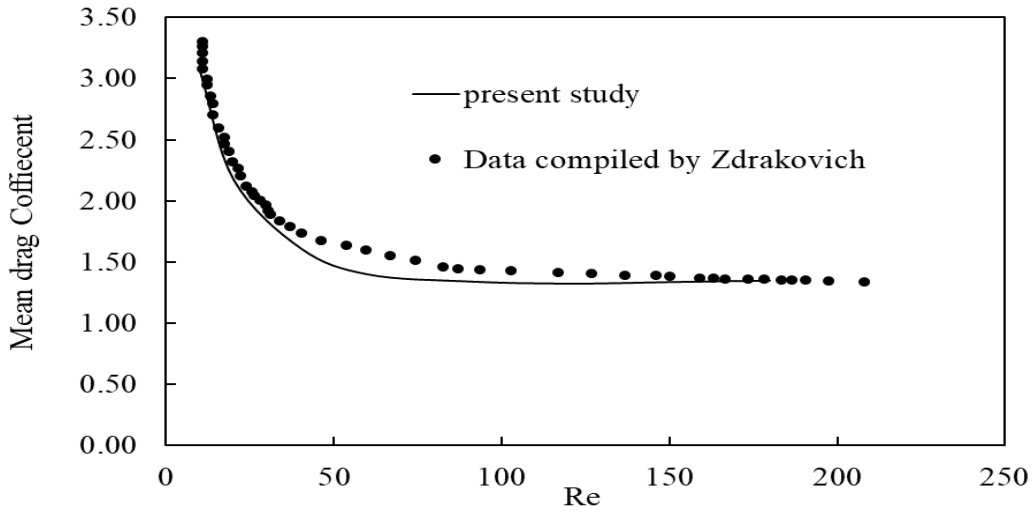

b

Fig. 3. Variations of a) Strouhal number and b) mean drag coefficient with Reynolds number.

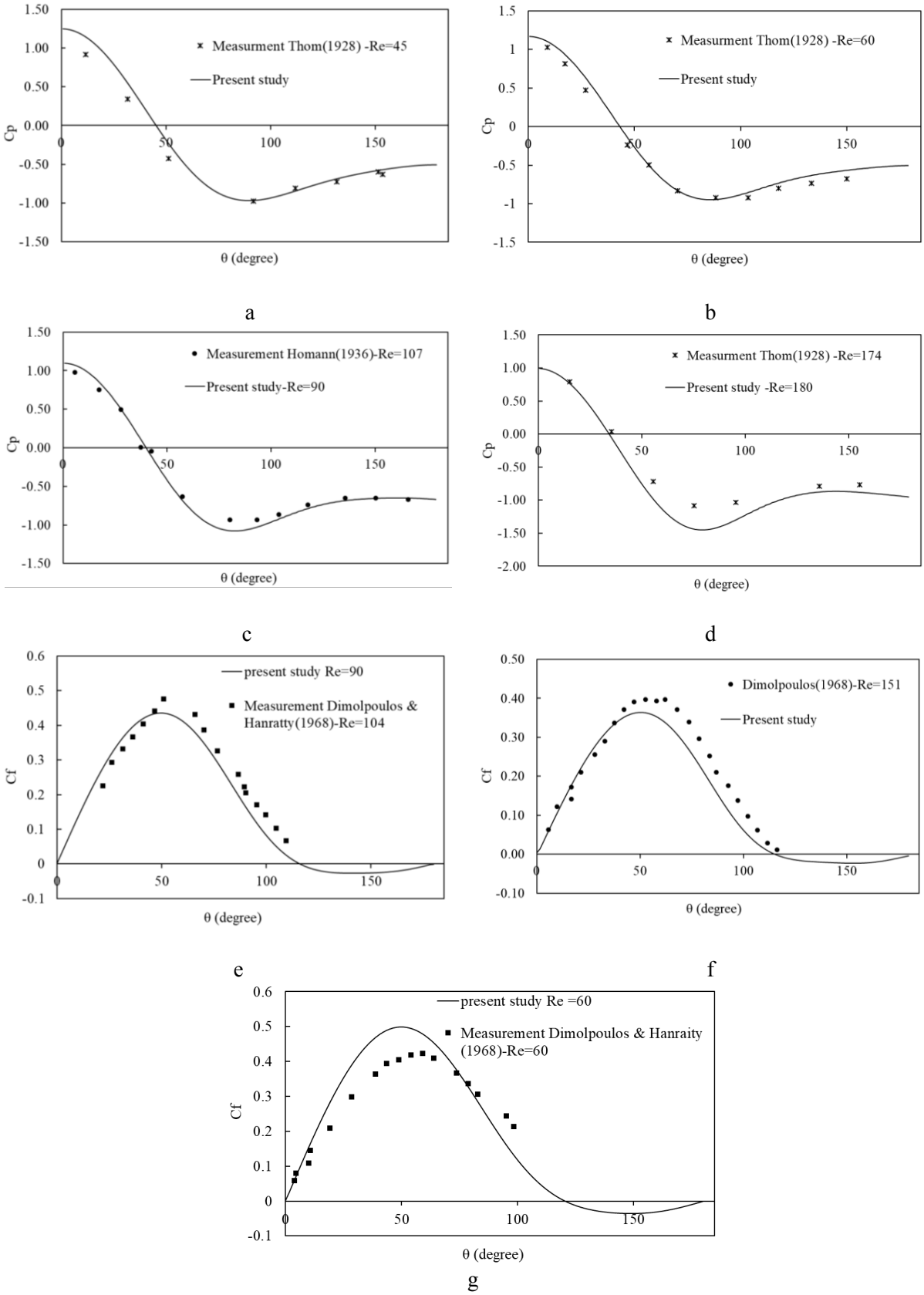

Fig. 4. Surface pressure and skin fraction coefficient on the circular cylinder surface, (a) surface pressure coefficient; Re =40, (b) surface pressure coefficient; Re =60, (c) surface pressure coefficient; Re =90, (d) surface pressure coefficient; Re =180, (e) skin friction coefficient; Re =90, (f) skin friction coefficient; Re=150, (g) skin friction coefficient; Re =60.

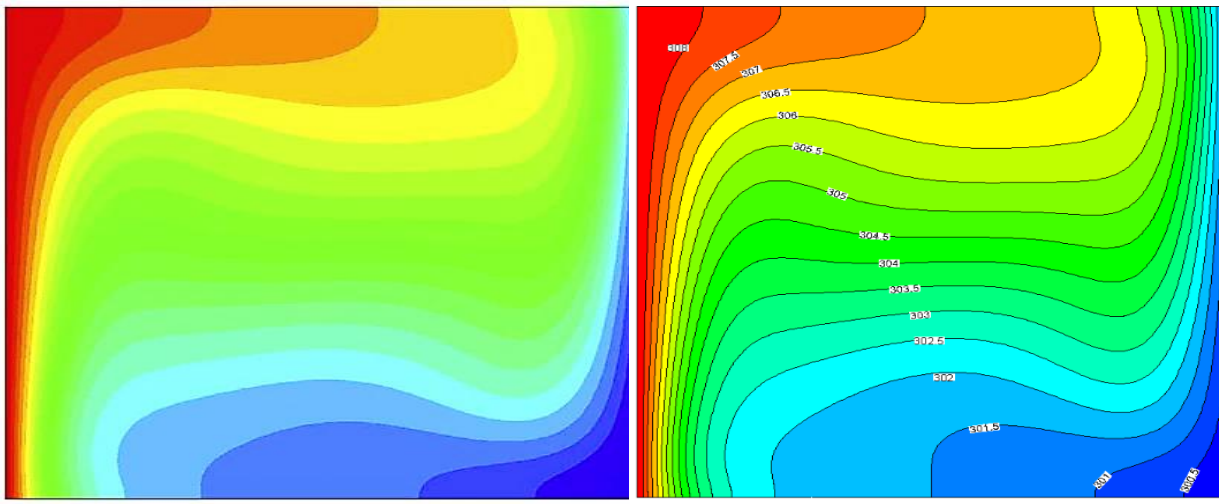

Fig. 5. Comparison between temperature field results done by the present code and those of the previous work; a) Song and Tagawa [49] b) present study

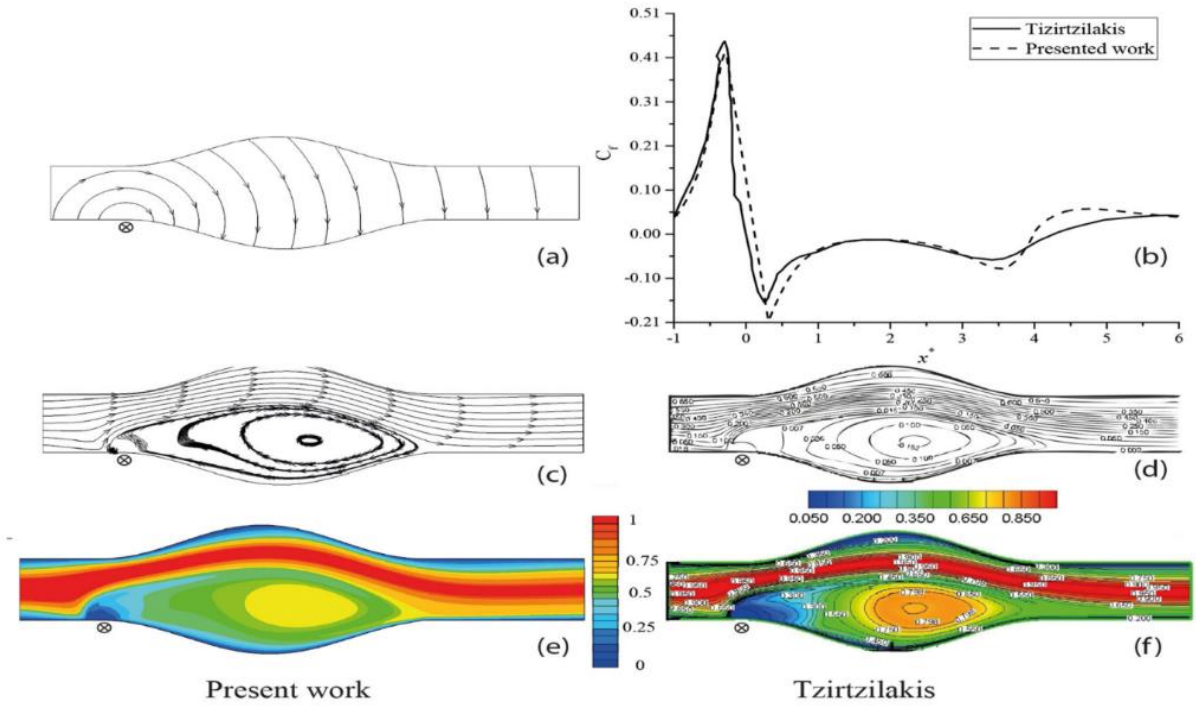

Fig. 6. Aneurysm flow for Re = 200, Mn = 328, single magnetic source (wire) (a): magnetic field strength contours, (b): wall shear stress distribution along lower wall, (c,d): Stream lines, (e,f): Temperature contours.

under the effect of the wire magnetic field (Tzirtzilakis [50]). Comparison of the contours of the magnetic field strength, local skin friction coefficient on the lower wall, flow streamlines, and isotherms for *Re*=200 and *Mn*=328 are presented in Fig. 6. As shown in Figs. 5 and 6, the results are in good agreement with other numerical studies. It should be mentioned that the main source of the errors obtained between the results rise from the experimental instrument uncertainty, empirical measurement and common numerical method errors. For further information about the validity of the code used in the current work, refer to the references of [38, 39, 51, 52].

3- Results and discussion

In this study, the effect of pure water and magnetic nanofluid (Fe_3O_4-water) injection on the flow and heat transfer

Table 3. Comparison of the average Nusselt number from the present study with the those of Zdravkovich [43].

Re	*Nu* (present)	*Nu* (Zdravkovich)	Error%
120	11.54	11.97	3.59
150	13.065	13.38	2.35
180	14.37	14.66	1.98

characteristics, such as drag coefficient, Nusselt number, and entropy generation in the presence and absence of magnetic field are investigated. For all cases, the results are evaluated for Reynolds number in the range of $120 \le Re \le 180$, nanoparticle volume fraction $0 \le \varphi \le 0.02$ and nanoparticle diameter 10 nm. Pure water is injected symmetrically in y direction with a velocity of 1/2 U from the gaps located at the top and bottom of the cylinder. Note that current carrier wire is fixed at the center of the cylinder and magnetic field intensity varies in the range of $0 \le B \le 0.0035$ T.

3- 1- Effect of pure water injection on drag coefficient, Nusselt number and entropy generation in absence of magnetic field

This section focuses on the injection of pure water from the cylinder surface in the absence of a magnetic field and its effect on flow and heat transfer. When blowing occurs, two secondary vortices form on both sides of the gaps according to Fig. 7. The presence of a certain amount of vorticity in the rear of the cylinder indicates the presence of strong recirculating flows. It is also observed that in the case of injection, this rear vorticity region approaches the surface of the cylinder. Due to the magnitude increment of vorticities by water injection, the static pressure defecte is higher in the case of blowing, which causes the drag coefficient increment.

To demonstrate the vortex shedding phenomenon instantly after the cylinder, a time cycle of the flow pattern is presented in Fig.8. Five flow shots of the domain in different dimensionless times are selected to prove the shedding after the cylinder. As seen, the stream function values and streamline configuration are the same in times of A and E which confirms the quasi-periodic behavior of the flow.

It is obvious from Fig. 9. that, the flow injection from gaps, causes to interruption and regeneration of the thermal boundary layer. Due to the boundary layer regeneration, its thickness becomes thinner and, as a result, the heat transfer coefficient and the average Nusselt number increase.

Table 4 shows the Nusselt number values for three Reynolds numbers of 120, 150 and 180, which increased by 16.85%, 13.51%, and 11.45%, respectively, due to fluid injection.

Values of drag coefficient are demonstrated in Table 4 for conditions with or without injection on a circular cylinder. As shown in Table 5, the vorticity magnitude increases with the injection of fluid from the top and bottom of the cylinder.

The formation of these vortices by flow injection and augmentation of vorticity magnitude causes energy loss in the fluid flow. As a result, according to Table 6, the thermal and frictional entropy generation increases. Although increasing the amount of entropy generation is undesirable, the main purpose of the present work is to reduce the drag coefficient of the circular cylinder.

3- 2- Effect of nanofluid injection on drag coefficient, Nusselt number and entropy generation in the presence and absence of magnetic field

To study nanoparticle volume fraction, in this section φ =0.01 and φ =0.02 are considered for three different Reynolds numbers of 120,150 and 180. Additionally, drag coefficient, Nusselt number, and entropy generation variations with or without magnetic effect have been reported for the constant diameter of nanoparticles 10 nm.

3- 2- 1- Results for nanofluid injection in the absence of magnetic field

By increasing the volume fraction of nanoparticles, the values of density, thermal conductivity, and dynamic viscosity increase. On the other hand, the increment of the density is more than the dynamic viscosity, therefore, the equivalent Reynolds numbers increase which results in a drag coefficient increment. The effects of adding nanoparticles on heat transfer at the circular cylinder surface are shown in Table 7 for three Reynolds numbers 120, 150, and 180. It can be seen that for all values of Reynolds number, increment of drag coefficient causes to reduction of the fluid momentum and hence the convection heat transfer. So, variation of volume fraction from 0 to 0.02 causes to about 11% augmentation of the drag coefficient and a reduction in Nusselt number, simultaneously. For Reynolds numbers of 120, 150, and 180 variation of volume fraction from 0% to 2% results in 3.38%, 2.09%, and 1.136% decrease in the Nusselt number, respectively. Changes of drag coefficient against time are presented in Fig.10 for different volume fractions of injected nanofluid.

Table 8 illustrates the changes in thermal, fluid friction, and total entropy generation by increasing the volume fraction

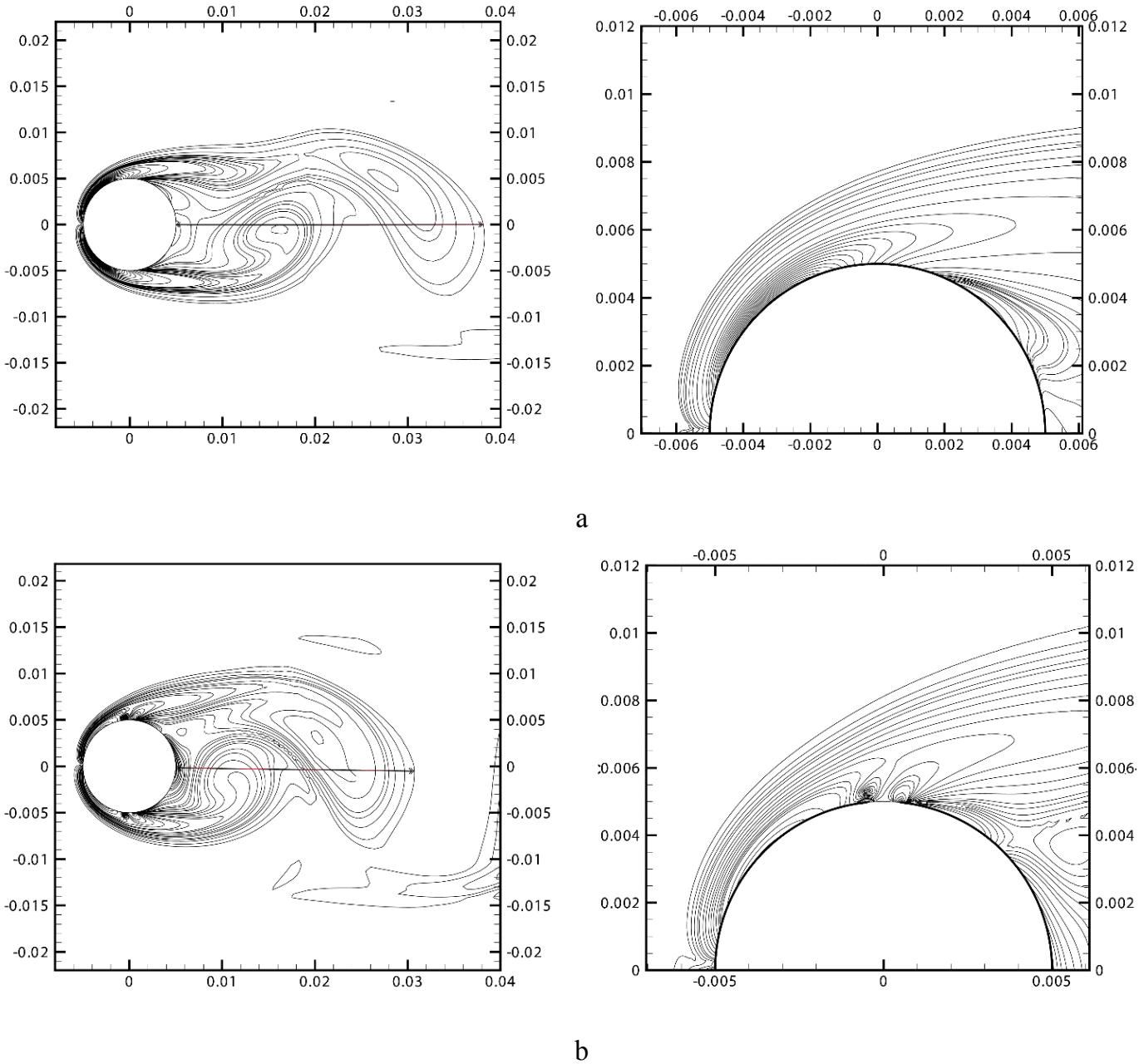

Fig. 7. Vorticity contours at the same phase at Re=180 a) Without injection and b) With injection.

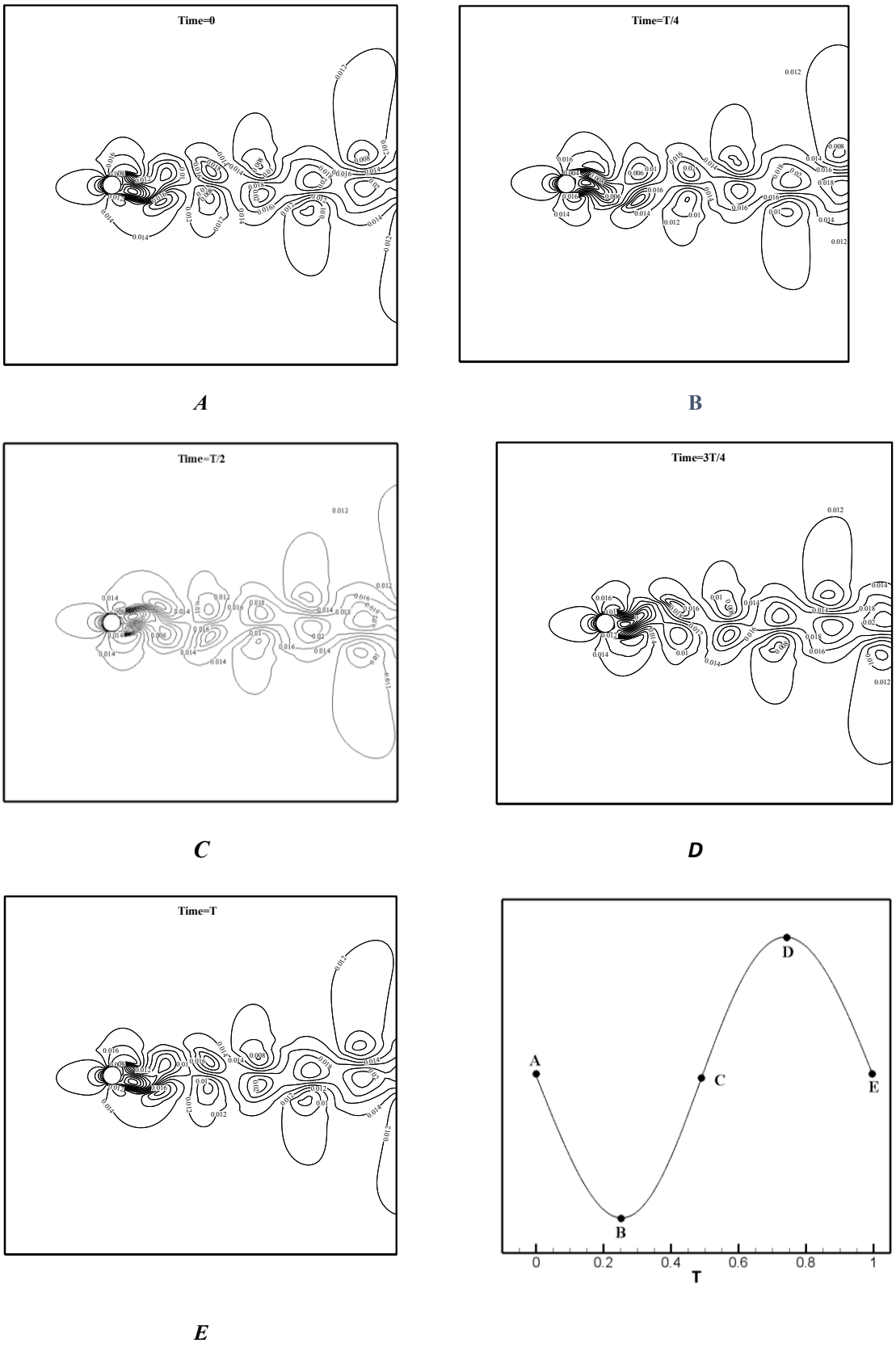

Fig. 8. Periodic flow pattern at Re=180 for corresponding points on a cycle of pure water injection flow

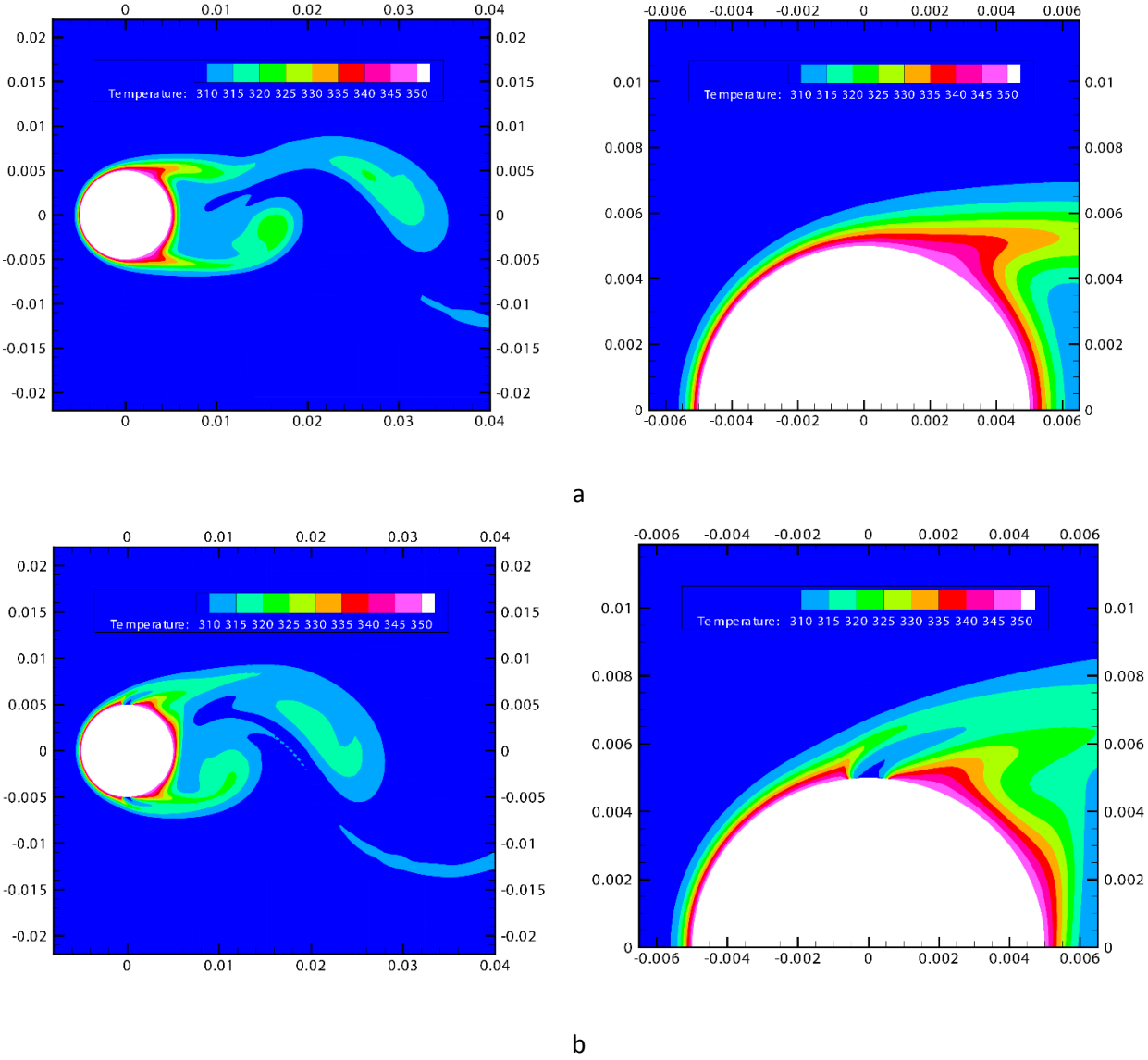

Fig. 9. Temperature contours at Re=180 a) Without injection and b) With injection.

Table 4. Variation of Cd and Nu for various Reynolds Numbers for conditions with and without pure water injection in the absence of magnetic field.

	Without injection		With injection	
Re	*Cd*	*Nu*	C_d	*Nu*
120	1.3265	11.54	1.3505	13.485
150	1.3395	13.065	1.3575	14.83
180	1.3505	14.37	1.3725	16.015

Table 5. Effect of nanofluid injection on the maximum magnitude of vorticities for different Reynolds numbers in the absence of magnetic field.

Re	maximum Magnitude of vorticity without injection	maximum Magnitude of vorticity with injection
120	19.9	40.7
150	29.2	51.4
180	39.7	66.9

Table 6. Variation of thermal and fluid friction and total entropy generation for conditions with and without injection at Reynolds180.

injection	S_t	S_F	S_T
NO	0.00293128	1.9141E-010	0.00293128
YES	0.00298699	2.43E-010	0.00298699

Table 7. Variation of the drag coefficient and average Nusselt number with the increase of volume fraction in Reynolds 120, 150 ,180 for B=0 T.

	Re=120		*Re*=150		*Re*=180	
φ	C_d	*Nu*	C_d	*Nu*	C_d	*Nu*
0	1.771	13.485	1.847	14.83	1.895	16.02
0.01	1.817	13.265	1.921	14.69	1.978	15.95
0.02	1.891	13.03	2.038	14.52	2.104	15.84

for Reynolds 180. As expected, it can be concluded that both thermal and fluid friction entropy generations are affected by the changes in thermal conductivity and equivalent Reynolds number. As mentioned before, the thermal conductivity of nanofluid increases up to 4.46% in the volume fraction of 0.02 which leads to enhancement of thermal entropy generation. Also, an increment of equivalent Reynolds number causes to increase in the fluid fraction entropy generation, however, the entropy generation due to heat transfer is dominant hence, Bejan number (*Be*), the ratio of thermal entropy generation to total entropy generation, is close to 1. The total entropy generation increases up to 5.89% for the volume fraction of 1% and 8.16% for the volume fraction of 2%. Table 9 shows the frictional and thermal entropy generation, in volume fraction of 0% for three Reynolds numbers 120, 150, and 180. As can be seen, the Reynolds number increase leads to the increment of fluid friction and thermal entropy generation amounts.

3- 2- 2- Results for nanofluid injection in the presence of magnetic field

Fig.11 and Fig.12 illustrate the changes of drag coefficient, against the magnetic field ($B = \mu_0 H_0 = \mu_0 I / (2\pi\lambda)$) at various volume fractions for three Reynolds numbers of 120, 150, and 180. It is obvious from the results that, by increasing the intensity of the magnetic field, the drag coefficient reduces. The variation of the maximum magnitude of the vorticities, the stagnation, and the base pressure coefficient, against the magnetic field for Reynolds 180 are presented in Table 10. According to the results, when the magnetic field (*B*) is 0.002

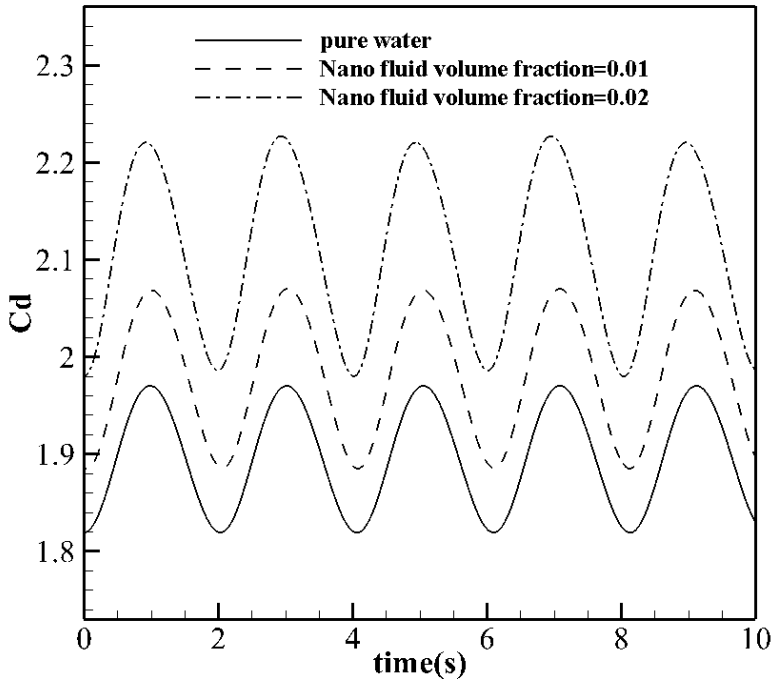

Fig. 10. Variation of drag coefficient against time on the cylinder surface at Re=180.

Table 8. Variation of thermal and fluid friction and total entropy generation in various volume fractions for Re=180.

φ	S_t	S_F	S_T
0	0.00298699	2.43E-010	0.00298699
0.01	0.00316278	2.67E-010	0.00316278
0.02	0.00323075	3.15E-010	0.00323075

Table 9. Variation of thermal, fluid friction, and total entropy generation in Reynolds numbers of 120, 150, and 180 for pure water fluid.

Re	S_t	S_F	S_T
120	0.00251133	7.48E-011	0.00251133
150	0.00278081	1.43E-010	0.00278081
180	0.00298699	2.43E-010	0.00298699

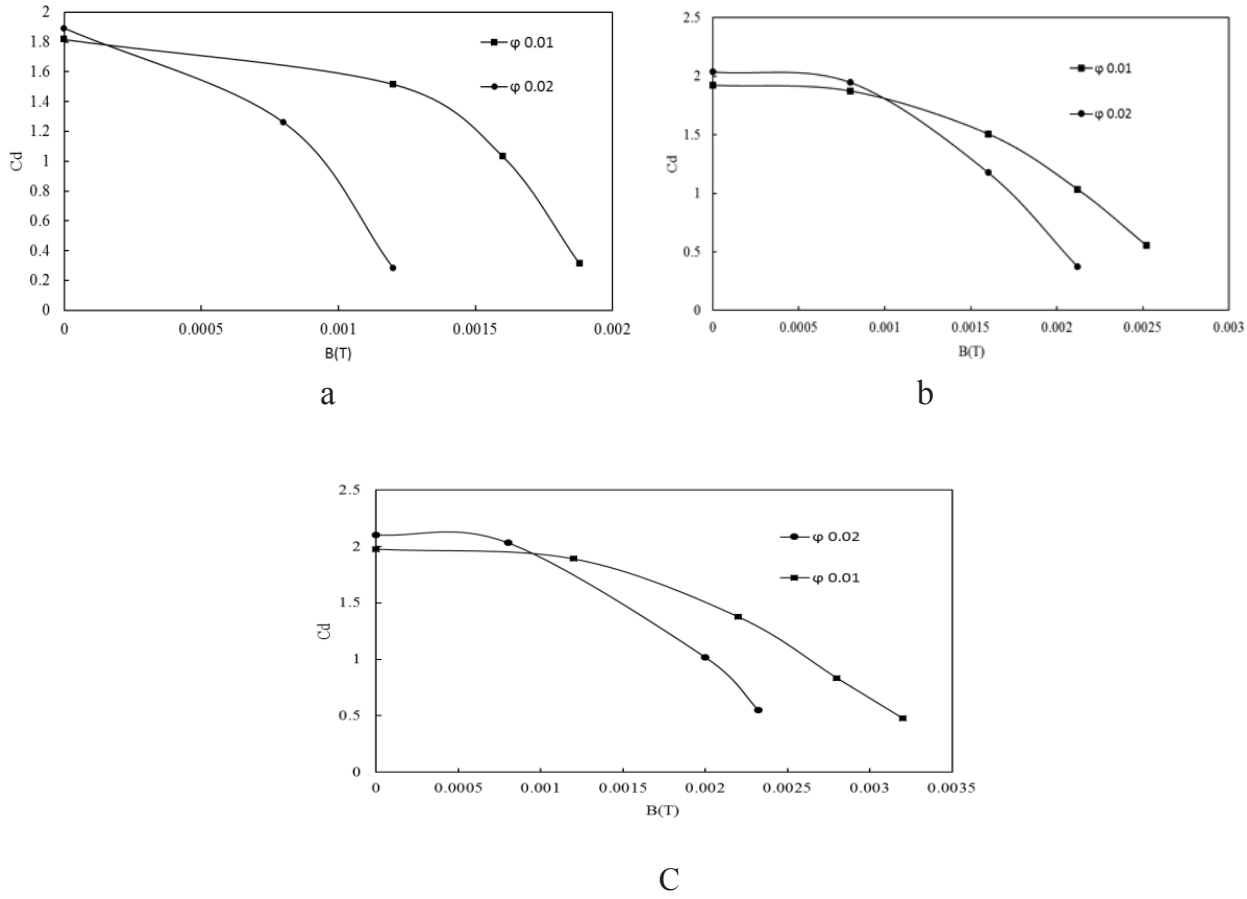

Fig. 11. Variations of mean drag coefficient against the intensity of magnetic field for Reynolds number a)120 b)150 c)180.

T the pressure drag coefficient reduces by about 153% against the no-magnetic field case. On the other hand, the previous works report lower reduction values in drag coefficient. For instance, Prabir et al. [16] report that there is 89.2% decrease in drag coefficient over a cylinder by inserting a rigid splitter at the backside of the cylinder. Additionally, Feng et al. [17] conducted 2D flow around a circular cylinder with a traveling wavy wall and concluded a maximum drag reduction of 78.35%. also, Gao et al. [18] experimentally studied the flow around a cylinder with suction/blowing structures on the surface of the cylinder and reported that the maximum drag reduction is about 13.68%. These comparisons reveal that the drag reduction mechanism presented in the current work is more efficient. Moreover, the variation of local skin friction and pressure coefficient is demonstrated in Fig.13. Regarding the results, the maximum magnitude of the vorticities and the differences between stagnation and base pressure coefficients decline, with the increment of the magnetic field.

To illustrate the further effectiveness of the magnetic field for higher volume fractions, a schematic of nanoparticles distribution around the cylinder surface for the volume fraction of 0.02 is shown in Fig.14 for Reynolds 150. It is evident from Fig.14 that by increasing the intensity of the magnetic field, due to overcoming of the magnetophoresis term relative to other terms, such as advection, thermophoresis, and Brownian diffusion, the concentration of nanoparticles increases in the behind of cylinder surface.

Variation of Kelvin force magnitude against of intensity of the magnetic field in θ=141° and volume fraction of 0.02 for *Re*=150 are presented in Fig. 15. It can be perceived that, at lower intensity of the magnetic field, the magnitude of Kelvin force is similar to the condition of the non-existence of the magnetic field. Moreover, by further incrementing the intensity of the Magnetic field, the Kelvin force increases. Therefore, the behind region of the cylinder surface is surrounded by the non-uniform layer of nanoparticles.

From the viewpoint of heat transfer modification, in the current study, the value of Nusselt number variation due to the effect of intensity of the magnetic field is affected by several parameters. Effective important parameters that influence the average Nusselt number value on the cylinder surface include the maximum magnitude of vorticities, conductivity of nanofluid, thermal boundary layer thickness, the density of nanofluid, dynamic viscosity of nanofluid

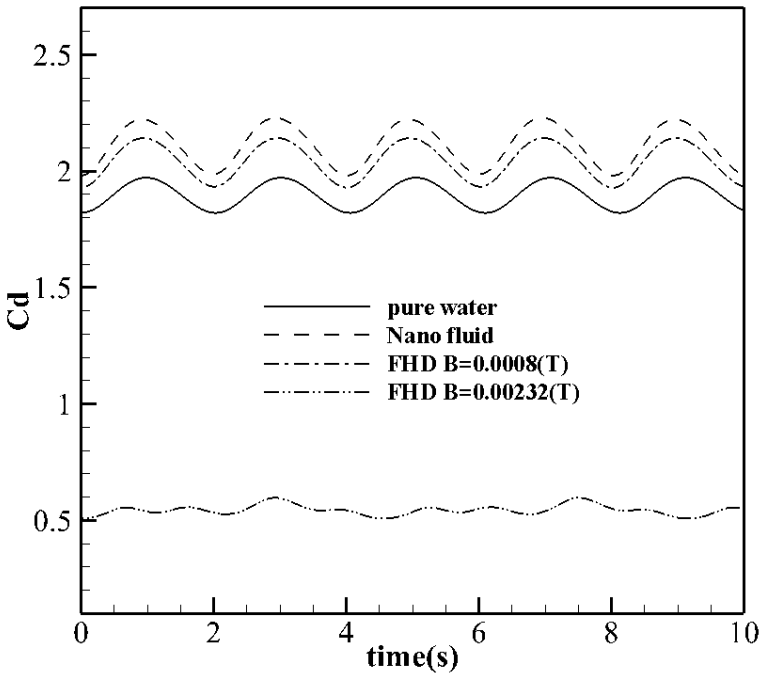

Fig. 12. Variation of drag coefficient against time on cylinder surface at Re=180 for different magnetic field.

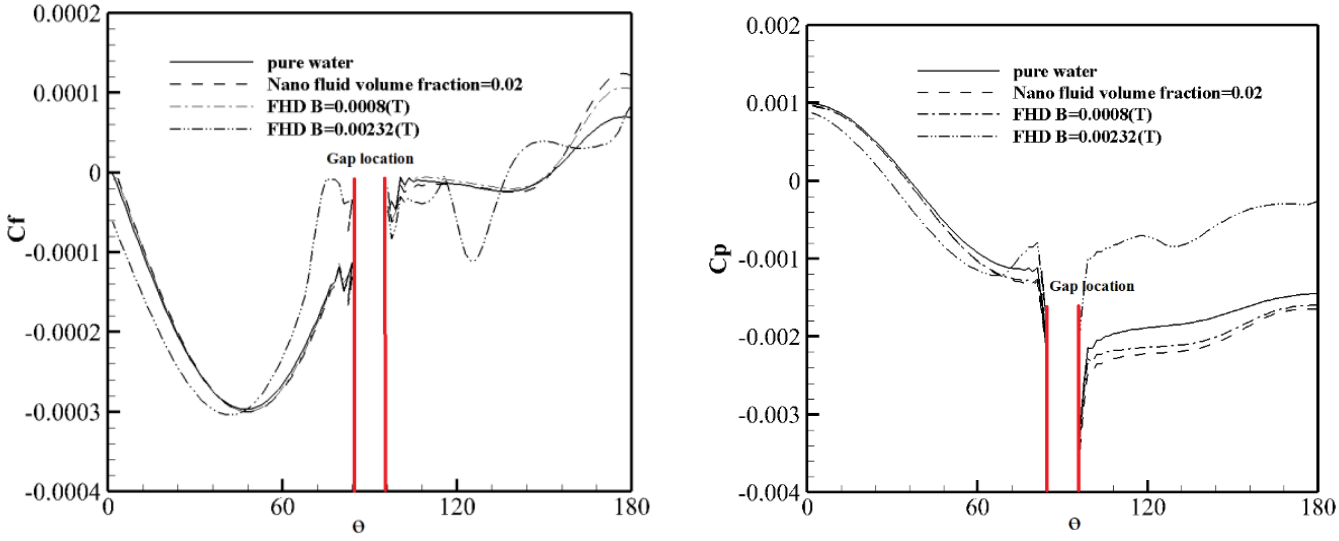

Fig. 13. Variation of local skin friction and pressure coefficient on cylinder surface at Re=180.

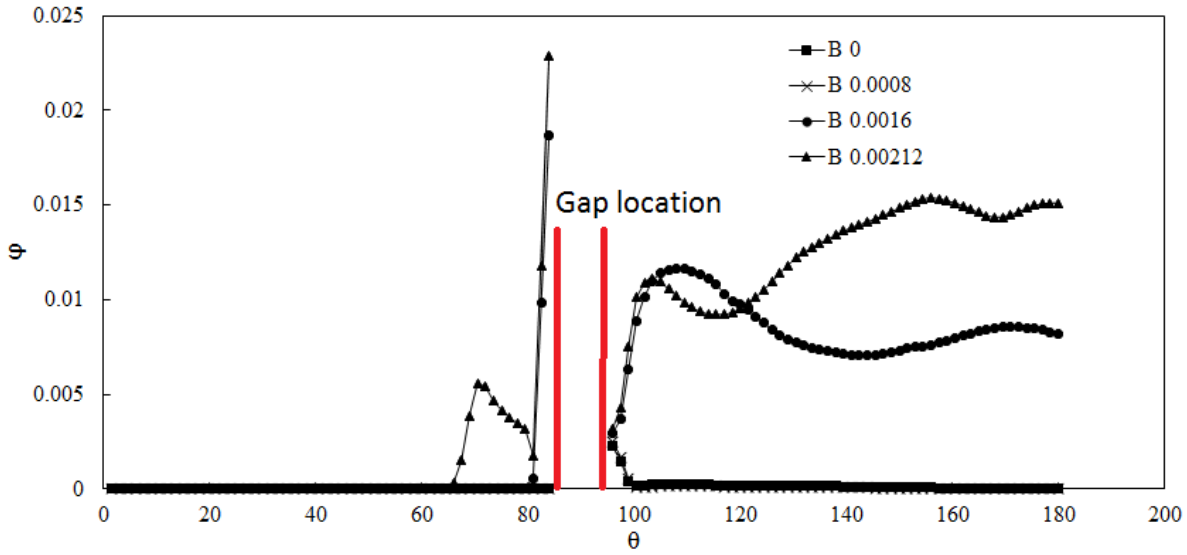

Fig. 14. Variation of nanoparticles concentration on the cylinder surface in Reynolds 150 and volume fraction of 0.02.

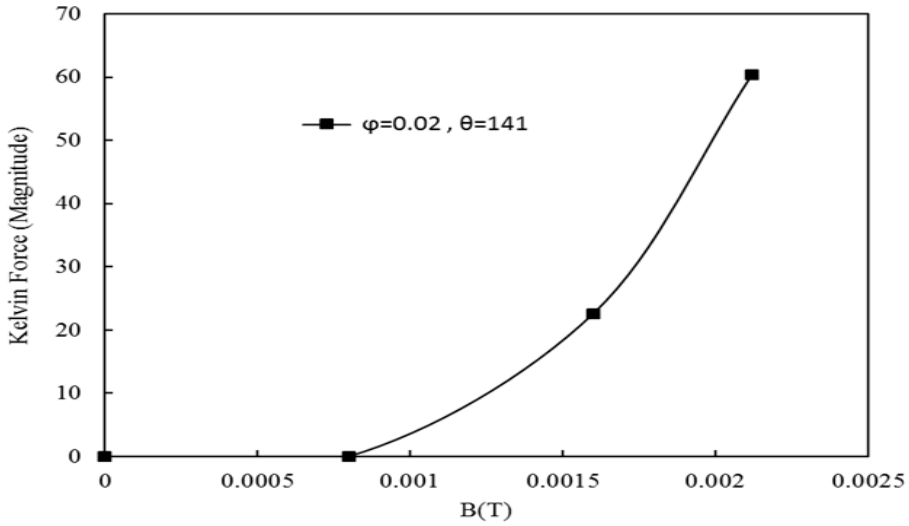

Fig. 15. Kelvin force magnitude in =141o changes against of magnetic field in Re=150.

and also equivalent Reynolds number. The fluctuations in Fig.16 at higher magnetic field intensities are due to the generation of vorticities and reattachment of flow. As illustrated in Table 10, it is irrefutable that, by increasing the intensity of the magnetic field the maximum magnitude of vorticity reduces dramatically which is the main reason for the decrement of the average Nusselt number. Furthermore, by the increment of the intensity of the magnetic field, the nanoparticle distribution becomes denser behind the cylinder surface increases that causes the local increment of thermal conductivity, density, and dynamic viscosity of nanofluid. It should be mentioned that the density of nanofluid increases more than Dynamic viscosity, therefore the average Nusselt number should increase. On the other hand, as shown in Fig. 17 the thermal boundary layer thickness increases which causes to the decline of the average Nusselt number. In low magnetic field intensities, the reduction of the Nusselt number is due to the enhancement of thermal boundary layer thicknesses

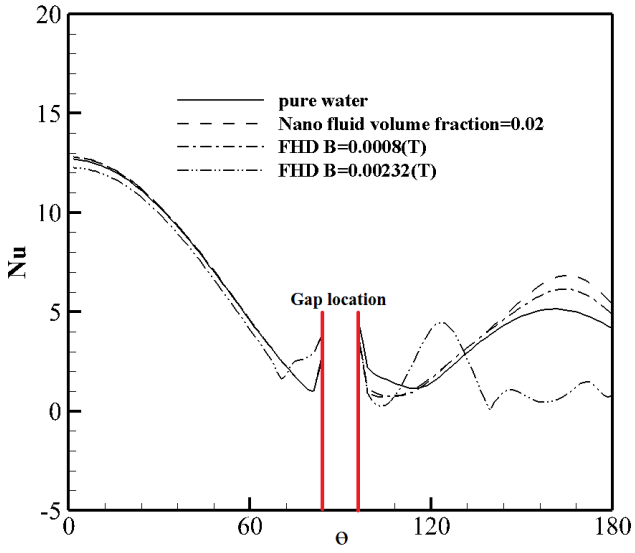

Fig. 16. Variation of local Nusselt number on cylinder surface at Re=180 for conditions

Table 10. The variation of the maximum magnitude of the vorticities, the stagnation, and base pressure coefficient, against the magnetic field for Reynolds number of 180.

B (T)	C_{p0}	C_{pb}	C_{p0}-C_{pb}	Vorticity magnitude
0	0.920635	-2.19942	3.120059	60.8
0.0008	0.949114	-2.10378	3.052894	58.8
0.002	0.962358	-0.86702	1.829375	51.5
0.00232	0.983856	-0.24312	1.226972	50

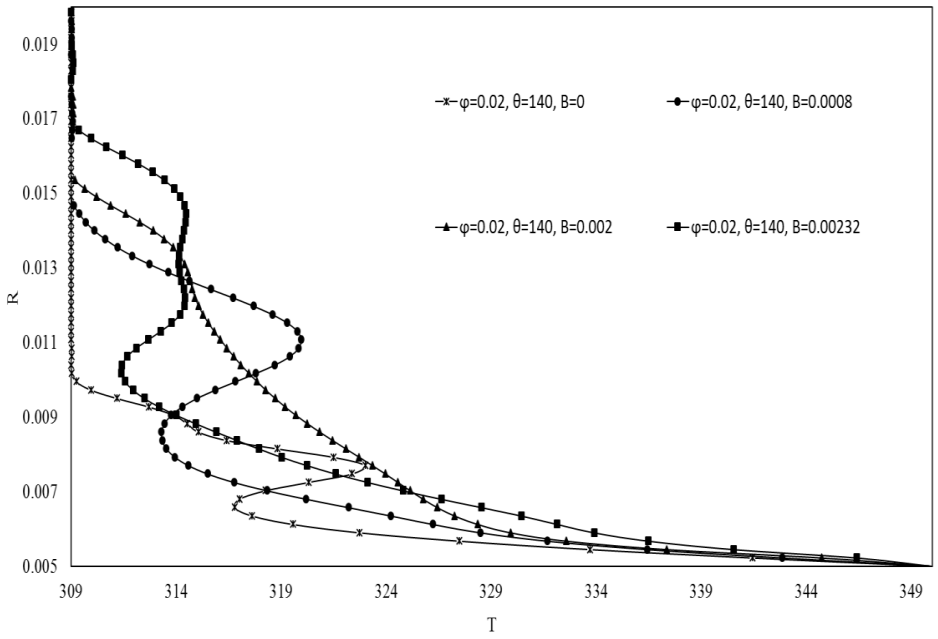

Fig. 17. Radial temperature variations for Re=180 at =140o.

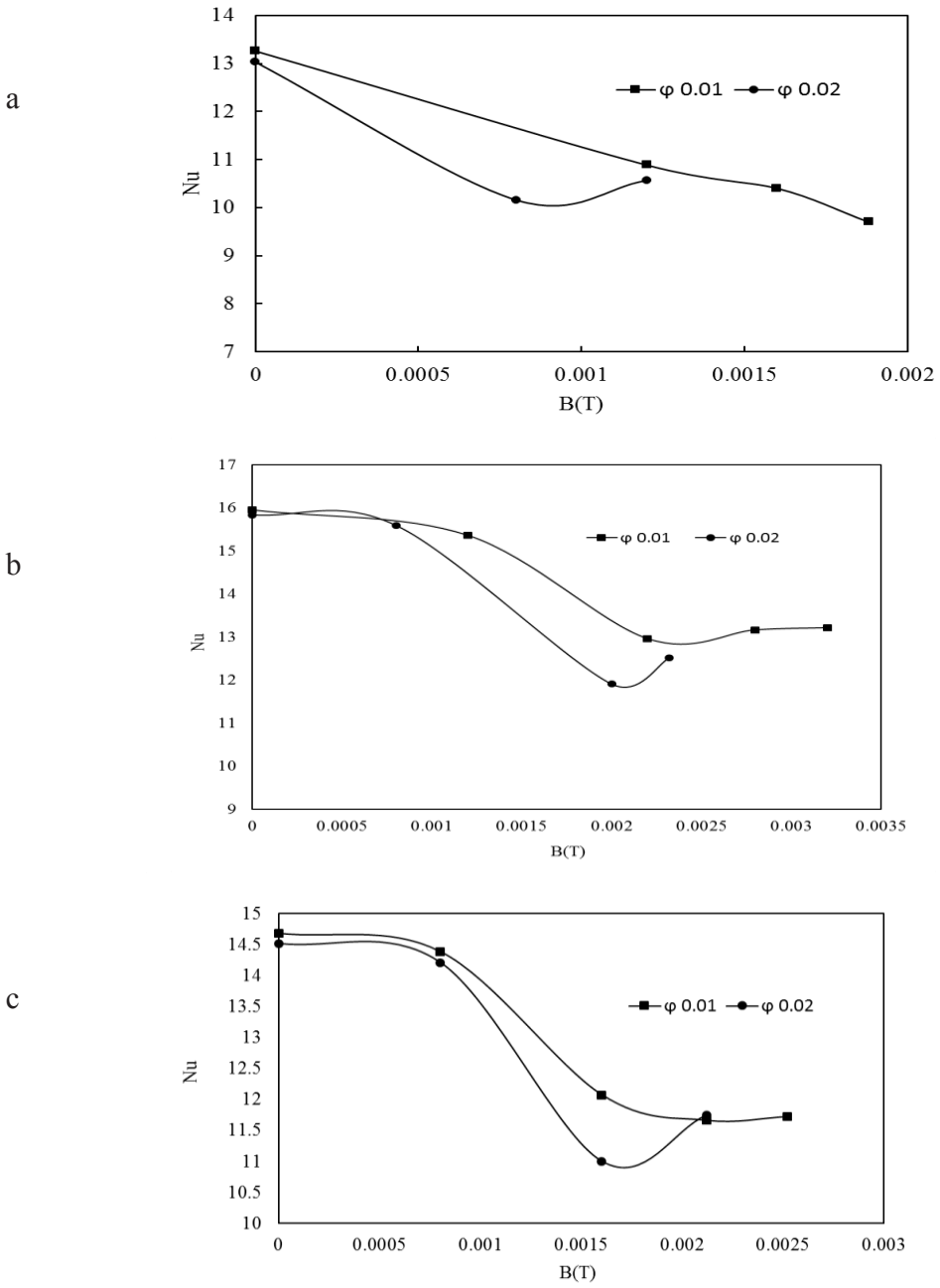

Fig. 18. Variations of average Nusselt number against the intensity of magnetic field for Reynolds numbers of a)120 b)150 c)180.

and the decrement of the maximum circulation magnitude of vorticities. However, in the higher intensity of the magnetic field, the effect of nanoparticles concentration behind the cylinder in the enhancement of equivalent Reynolds number and thermal conductivity of nanofluid overcomes to the other parameters.

Entropy generation is a factor by which system efficiency can be judged by that. So, it is necessary to identify the parameters affecting the increment of entropy generation. Table 11 shows the variations of entropy generation for volume fraction 0.02 and *Re*=180 in various intensity of the magnetic fields. Regarding the deterrent role of the Kelvin force, fluid friction entropy generation increases by the enhancement of magnetic field intensity. Thermal entropy generation as like as the obtained values for the Nusselt number decreases by increasing the intensity of the magnetic field up to 0.00232 and then increases by a further increment of the magnetic field. Also, it can be realized from the results that values of fluid friction entropy generation in comparison to thermal entropy generation can be neglected.

Table 11. Variation of thermal, fluid friction, and total entropy generation with Re=180 and ϕ=0.02 by increasing the intensity of magnetic field.

B (T)	S_t	S_F	S_T
0	0.00323075	3.15E-010	0.00323075
0.0008	0.00321085	3.11E-010	0.00321085
0.002	0.00289287	3.24E-010	0.00289287
0.00232	0.00293462	3.81E-010	0.00293462

Entropy generation reduction is desirable for industry and manufacturing new systems, therefore, utilizing the Kelvin force for minimization of entropy generation is efficient for industrial purposes.

4- Conclusion

A numerical simulation has been done by using a Boungiorno two-phase model and ferrohydrodynamics principles to study the effects of Fe_3O_4 / H_2O nanofluid on fluid flow and heat transfer around a circular cylinder in the presence of a magnetic field. In this study, the effects of the magnetic field and Nanoparticle volume fraction on the flow and heat transfer characteristics such as drag coefficient, Strouhal number, Nusselt number, the maximum magnitude of vorticities and entropy generation has been investigated. The most important obtained results are highlighted as follows:

In the case of no magnetic field, flow blowing from injection gaps by y component velocity ($v = U / 2$) causes to increment of drag coefficient and Nusselt number.

In Reynolds 120,150 and 180, in the absence of the magnetic field, with increasing the volume fraction from 0 to 0.02, the drag coefficient intensifies by about 11%.

For Reynolds numbers of 120, 150, and 180 by variation of volume fraction from 0% to 2%, the Nusselt number decreases 3.38%, 2.09%, and 1.136%, respectively.

when the magnetic field (B) is 0.002 T the pressure drag coefficient reduces by about 153% against the no-magnetic field case.

In Reynolds 120,150 and 180, with the increasing magnetic field, the drag coefficient reduces due to the reduction of the maximum magnitude of the vorticities and the pressure difference between the front and back of the cylinder.

In Reynolds 120,150 and 180, with the increasing magnetic field, total entropy generation, and Nusselt number decrease. Although their values increase by further enhancement of the intensity of the magnetite field.

For all under investigation cases, values of fluid friction entropy generation are so lower than values of thermal entropy generation.

All in all, the results of the current study demonstrate the efficiency of the utilization of Kelvin force in the reduction of drag coefficient and entropy generation of Fe_3O_4 / H_2O nanofluid. However, utilizing this method has its own challenges such as: embedding a nanofluid reservoir inside the cylinder, considering a pump, considering a check valve in the injection circuit to prevent the opposite flow of water into the nanofluid reservoir, etc.

Nomenclatures

D_T	Brownian diffusion coefficient, kg $m^{-1}s^{-1}$
d_p	diameter of the nanoparticle, m
D_T	thermophoresis diffusivity coefficient, kg $m^{-1}s^{-1}$
D	Diameter of circular Cylinder, m
B	Magnetic field, T
H	Magnetic field intensity
$\mathbf{J}_p$	particle flux vector, kg $m^{-2}s^{-1}$
M	Magnetization
k_B	Boltzmann's constant = 1.3806503× 10^{-23}J K^{-1}
$L(\xi)$	Langevin function
ξ	Langevin parameter
p	Pressure
Re	Reynolds number
T	Temperature, K
$\mathbf{V}$	velocity vector, ms^{-1}
x, y	Cartesian coordinates, m
f	Frequency, s^{-1}
μ_0	Permeability of vacuum
t	Time, s
T	Period of fluctuations, s
C_p	Drag coefficient
Nu	Nusselt number
C_l	Lift coefficient
St	Strouhal number
S_{gen}'''	Volumetric entropy generation

Sc	Schmidt Number
Mn	Magnetic Number
N_{BT}	diffusivity ratio parameter
C_f	Friction coefficient
C_p	Pressure coefficient
τ_w	Wall shear stress
F_d	Drag force, N
F_l	Lift force, N
MHD	Magneto Hydrodynamic
FHD	Ferro Hydro Dynamic

Greek symbols

μ	dynamic viscosity, kg $m^{-1}s^{-1}$
ρ	density, kg m^{-3}
ν	kinematic viscosity, m^2s^{-1}
θ	Angle
φ	volume fraction

Subscripts

f	base fluid
np	Particle
nf	nanofluid
t	thermal
F	Fluid friction

References

[1] A.A. Asadi, M.M. Heyhat, Study of using nanofluid in shell and tube heat exchangers with different sizes, Modares Mechanical Engineering, 17(3) (2017) 455-458.

[2] M. Farrokh, T. Goodarz, J. Samad, N. Javid, H. Amin, Analysis of Entropy Generation of a Magneto-Hydrodynamic Flow Through the Operation of an Unlooped Pulsating Heat Pipe, Journal of Heat Transfer, 140(8) (2018) 082801.

[3] S. Jafarmadar, N. Azizinia, N. Razmara, F. Mobadersani, Thermal analysis and entropy generation of pulsating heat pipes using nanofluids, Applied Thermal Engineering, 103 (2016) 356-364.

[4] M. Pantzali, A. Mouza, S. Paras, Investigating the efficacy of nanofluids as coolants in plate heat exchangers (PHE), Chemical Engineering Science, 64(14) (2009) 3290-3300.

[5] H.R.T. Bahrami, S. Zareie, H. Saffari, A numerical analysis of dropwise condensation of nanofluid on an inclined flat plate, Modares Mechanical Engineering, 17(3) (2017) 105-114.

[6] P.S. Ayyaswamy, V. Muzykantov, D.M. Eckmann, R. Radhakrishnan, Nanocarrier hydrodynamics and binding in targeted drug delivery: challenges in numerical modeling and experimental validation, Journal of nanotechnology in engineering and medicine, 4(1) (2013) 011001.

[7] K.M. Pondman, N.D. Bunt, A.W. Maijenburg, R.J. van Wezel, U. Kishore, L. Abelmann, J.E. ten Elshof, B. ten Haken, Magnetic drug delivery with FePd nanowires, Journal of Magnetism and Magnetic Materials, 380 (2015) 299-306.

[8] A. Sharifi, S. Yekani Motlagh, H. Badfar, Investigation of the effects of two parallel wires' non-uniform magnetic field on heat and biomagnetic fluid flow in an aneurysm, International Journal of Computational Fluid Dynamics, 32(4-5) (2018) 248-259.

[9] J.-M. Shen, F.-Y. Gao, T. Yin, H.-X. Zhang, M. Ma, Y.-J. Yang, F. Yue, cRGD-functionalized polymeric magnetic nanoparticles as a dual-drug delivery system for safe targeted cancer therapy, Pharmacological Research, 70(1) (2013) 102-115.

[10] T.-H. Tsai, R. Chein, Performance analysis of nanofluid-cooled microchannel heat sinks, International Journal of Heat and Fluid Flow, 28(5) (2007) 1013-1026.

[11] J.P. Dulhani, S. Sarkar, A. Dalal, Effect of angle of incidence on mixed convective wake dynamics and heat transfer past a square cylinder in cross flow at Re= 100, International Journal of Heat and Mass Transfer, 74 (2014) 319-332.

[12] H. Bayat, M. Majidi, M. Bolhasani, A.K. Alilou, A.M. Lavasani, Unsteady flow and heat transfer of nanofluid from circular tube in cross-flow, International Journal of Aerospace and Mechanical Engineering, 9(12) (2015) 2086-2091.

[13] A.P.S. Bhinder, S. Sarkar, A. Dalal, Flow over and forced convection heat transfer around a semi-circular cylinder at incidence, International journal of heat and mass transfer, 55(19-20) (2012) 5171-5184.

[14] M.S. Valipour, R. Masoodi, S. Rashidi, M. Bovand, M. Mirhosseini, A numerical study on convection around a square cylinder using Al2O3-H2O nanofluid, Thermal science, 18(4) (2014) 1305-1314.

[15] M. Bovand, S. Rashidi, J. Esfahani, Enhancement of heat transfer by nanofluids and orientations of the equilateral triangular obstacle, Energy conversion and management, 97 (2015) 212-223.

[16] P. Sikdar, S.M. Dash, K.P. Sinhamahapatra, A numerical study on the drag reduction and wake regime control of the tandem circular cylinders using splitter plates, Journal of Computational Science, 66 (2023) 101927.

[17] F. Xu, W.-L. Chen, W.-F. Bai, Y.-Q. Xiao, J.-P. Ou, Flow control of the wake vortex street of a circular cylinder by using a traveling wave wall at low Reynolds number, Computers & Fluids, 145 (2017) 52-67.

[18] D. Gao, G. Chen, W. Chen, Y. Huang, H. Li, Active control of circular cylinder flow with windward suction and leeward blowing, Experiments in Fluids, 60 (2019) 1-17.

[19] P. Joseph, X. Amandolese, C. Edouard, J.-L. Aider, Flow control using MEMS pulsed micro-jets on the Ahmed body, Experiments in fluids, 54 (2013) 1-12.

[20] S. Kunze, C. Brücker, Control of vortex shedding on a circular cylinder using self-adaptive hairy-flaps, Comptes Rendus Mécanique, 340(1-2) (2012) 41-56.

[21] K. Muralidharan, S. Muddada, B. Patnaik, Numerical simulation of vortex induced vibrations and its control by suction and blowing, Applied Mathematical Modelling, 37(1-2) (2013) 284-307.

[22] G. Nati, M. Kotsonis, S. Ghaemi, F. Scarano, Control of vortex shedding from a blunt trailing edge using plasma actuators, Experimental Thermal and fluid science, 46 (2013) 199-210.

[23] G. Ozkan, H. Akilli, Flow control around bluff bodies by attached permeable plates, International Journal of Mechanical and Mechatronics Engineering, 8(5) (2014) 1036-1040.

[24] S. Mittal, A. Raghuvanshi, Control of vortex shedding behind circular cylinder for flows at low Reynolds numbers, International journal for numerical methods in fluids, 35(4) (2001) 421-447.

[25] B. Zhou, X. Wang, W.M. Gho, S.K. Tan, Force and flow characteristics of a circular cylinder with uniform surface roughness at subcritical Reynolds numbers, Applied Ocean Research, 49 (2015) 20-26.

[26] W.-L. Chen, D.-B. Xin, F. Xu, H. Li, J.-P. Ou, H. Hu, Suppression of vortex-induced vibration of a circular cylinder using suction-based flow control, Journal of Fluids and Structures, 42 (2013) 25-39.

[27] J.C. Schulmeister, J. Dahl, G. Weymouth, M. Triantafyllou, Flow control with rotating cylinders, Journal of Fluid Mechanics, 825 (2017) 743-763.

[28] D. Grigoriadis, I. Sarris, S.C. Kassinos, MHD flow past a circular cylinder using the immersed boundary method, Computers & Fluids, 39(2) (2010) 345-358.

[29] H. Zhang, B.-c. Fan, Z.-h. Chen, H.-z. Li, Numerical study of the suppression mechanism of vortex-induced vibration by symmetric Lorentz forces, Journal of Fluids and Structures, 48 (2014) 62-80.

[30] M.R. Rezaie, M. Norouzi, Numerical investigation of MHD flow of non-Newtonian fluid over confined circular cylinder: a lattice Boltzmann approach, Journal of the Brazilian Society of Mechanical Sciences and Engineering, 40 (2018) 1-10.

[31] H. Aminfar, M. Mohammadpourfard, Y.N. Kahnamouei, A 3D numerical simulation of mixed convection of a magnetic nanofluid in the presence of non-uniform magnetic field in a vertical tube using two phase mixture model, Journal of Magnetism and Magnetic Materials, 323(15) (2011) 1963-1972.

[32] M. Bahiraei, M. Hangi, Investigating the efficacy of magnetic nanofluid as a coolant in double-pipe heat exchanger in the presence of magnetic field, Energy Conversion and Management, 76 (2013) 1125-1133.

[33] M. Mahmoudi, S. Sant, B. Wang, S. Laurent, T. Sen, Superparamagnetic iron oxide nanoparticles (SPIONs): development, surface modification and applications in chemotherapy, Advanced drug delivery reviews, 63(1-2) (2011) 24-46.

[34] I. Sharifi, H. Shokrollahi, S. Amiri, Ferrite-based magnetic nanofluids used in hyperthermia applications, Journal of magnetism and magnetic materials, 324(6) (2012) 903-915.

[35] S. Shuchi, K. Sakatani, H. Yamaguchi, An application of a binary mixture of magnetic fluid for heat transport devices, Journal of magnetism and magnetic materials, 289 (2005) 257-259.

[36] S. Yekani Motlagh, M. Mehdizadeh Youshanloei, T. Safabakhsh, Numerical investigation of FHD pump for pumping the magnetic nanofluid inside the microchannel with hydrophobic walls, Journal of the Brazilian Society of Mechanical Sciences and Engineering, 41 (2019) 1-16.

[37] S. Yekani Motlagh, S. Deyhim, Numerical simulation of magnetic nanoparticle delivery at location of abdominal aortic bifurcation using single wire magnetic source, Modares Mechanical Engineering, 17(9) (2017) 65-74.

[38] A. Sharifi, S.Y. Motlagh, H. Badfar, Ferro hydro dynamic analysis of heat transfer and biomagnetic fluid flow in channel under the effect of two inclined permanent magnets, Journal of Magnetism and Magnetic Materials, 472 (2019) 115-122.

[39] A. Sharifi, S.Y. Motlagh, H. Badfar, Numerical investigation of magnetic drug targeting using magnetic nanoparticles to the Aneurysmal Vessel, Journal of Magnetism and Magnetic Materials, 474 (2019) 236-245.

[40] J. Buongiorno, Convective transport in nanofluids, (2006).

[41] H.C. Brinkman, The viscosity of concentrated suspensions and solutions, The Journal of chemical physics, 20(4) (1952) 571-571.

[42] K. Khanafer, K. Vafai, M. Lightstone, Buoyancy-driven heat transfer enhancement in a two-dimensional enclosure utilizing nanofluids, International journal of heat and mass transfer, 46(19) (2003) 3639-3653.

[43] M. Zdravkovich, P. Bearman, Flow around circular cylinders—Volume 1: Fundamentals, Oxford University Press, 1997.

[44] C. Norberg, Pressure forces on a circular cylinder in cross flow, in: Bluff-Body Wakes, Dynamics and Instabilities: IUTAM Symposium, Göttingen, Germany September 7–11, 1992, Springer, 1993, pp. 275-278.

[45] C. Williamson, The natural and forced formation of spot-like 'vortex dislocations' in the transition of a wake, Journal of Fluid Mechanics, 243 (1992) 393-441.

[46] F. Homann, Influence of higher viscosity on flow around cylinder, Forschung aus dem Gebiete des Ingenieiuwesen, 17 (1936) 1-10.

[47] H.G. Dimopoulos, T.J. Hanratty, Velocity gradients at the wall for flow around a cylinder for Reynolds numbers between 60 and 360, Journal of Fluid Mechanics, 33(2) (1968) 303-319.

[48] A. Žukauskas, Heat transfer from tubes in crossflow, in: Advances in heat transfer, Elsevier, 1972, pp. 93-160.

[49] K.W. Song, T. Tagawa, Thermomagnetic convection of oxygen in a square enclosure under non-uniform magnetic field, International Journal of Thermal Sciences, 125 (2018) 52-65.

[50] E. Tzirtzilakis, Biomagnetic fluid flow in an aneurysm using ferrohydrodynamics principles, Physics of Fluids, 27(6) (2015).

[51] H. Badfar, S.Y. Motlagh, A. Sharifi, Study of blood flow inside the stenosis vessel under the effect of solenoid magnetic field using ferrohydrodynamics principles, The European Physical Journal Plus, 132 (2017) 1-13.

[52] S.Y. Motlagh, H. Soltanipour, Natural convection of Al2O3-water nanofluid in an inclined cavity using

Buongiorno's two-phase model, International Journal of Thermal Sciences, 111 (2017) 310-320.

HOW TO CITE THIS ARTICLE
S. Yekani Motlagh, I. Tolouie, E. Tolouie, F. Mobadersani, Ferrofluid Injection and Applied Magnetic Field Influences on the Characteristics of Flow Over a Cylinder, AUT J. Mech Eng., 7(2) (2023) 131-154.

DOI: 10.22060/ajme.2023.21980.6051